Geophysical Research Letters

RESEARCH LETTER
10.1029/2019GL082523

Observations and Modeling of a Hydrothermal Plume in Yellowstone Lake

Robert A. Sohn[1], Karen Luttrell[2], Emily Shroyer[3], Christian Stranne[4], Robert N. Harris[3], and Julia E. Favorito[3]

[1]Woods Hole Oceanographic Institution, Woods Hole, MA, USA, [2]Department of Geology and Geophysics, Louisiana State University and A. & M. College, Baton Rouge, LA, USA, [3]College of Earth, Ocean, and Atmospheric Sciences, Oregon State University, Corvallis, OR, USA, [4]Department of Geological Sciences, Stockholm University, Stockholm, Sweden

Key Points:
- Vertical velocity and conductivity-temperature-depth profiles reveal a hydrothermal plume in Yellowstone Lake
- The plume neutral buoyancy level is ~70 m above the lake floor, and vertical velocities of up to ~10 cm/s were observed in the mid-water column
- We estimate the plume has a total heat flux of ~28 MW

Supporting Information:
- Supporting Information S1
- Figure S1
- Figure S2
- Figure S3
- Figure S4
- Figure S5

Correspondence to:
R. A. Sohn,
rsohn@whoi.edu

Citation:
Sohn, R. A., Luttrell, K., Shroyer, E., Stranne, C., Harris, R. N., & Favorito, J. E. (2019). Observations and modeling of a hydrothermal plume in Yellowstone Lake. *Geophysical Research Letters*, *46*, 6435–6442. https://doi.org/10.1029/2019GL082523

Received 19 FEB 2019
Accepted 1 MAY 2019
Accepted article online 9 MAY 2019
Published online 22 JUN 2019

Abstract Acoustic Doppler current profiler and conductivity-temperature-depth data acquired in Yellowstone Lake reveal the presence of a buoyant plume above the "Deep Hole" hydrothermal system, located southeast of Stevenson Island. Distributed venting in the ~200 × 200-m hydrothermal field creates a plume with vertical velocities of ~10 cm/s in the mid-water column. Salinity profiles indicate that during the period of strong summer stratification the plume rises to a neutral buoyancy horizon at ~45-m depth, corresponding to a ~70-m rise height, where it generates an anomaly of ~5% (−0.0014 psu) relative to background lake water. We simulate the plume with a numerical model and find that a heat flux of 28 MW reproduces the salinity and vertical velocity observations, corresponding to a mass flux of 1.4×10^3 kg/s. When observational uncertainties are considered, the heat flux could range between 20 to 50 MW.

1. Introduction

Hydrothermal plumes are observed above deep-sea vent fields on mid-ocean ridges, where they play an important role in the detection/location of seafloor vents and provide estimates of the thermal and chemical fluxes of individual vent fields (e.g., Baker et al., 1995). By contrast, hydrothermal plumes in lacustrine environments have received relatively little attention despite the fact that hydrothermal vents have been documented in several lakes around the world, including in Lake Taupo in New Zealand (de Ronde et al., 2002), Lake Tanganyika in the East African Rift (Tiercelin et al., 1993), Lake Baikal in Siberia (Crane et al., 1991), Crater Lake in Oregon (Dymond et al., 1989), and Yellowstone Lake in Wyoming (Klump et al., 1988). To our knowledge, the only description of a lacustrine plume was made in a karstic lake (Lake Banyoles, Catalonia, Spain) where subterranean springs discharge fluids with a weak thermal anomaly that generate a small plume that rises ~18 m above the lake floor (Colomer et al., 2001; Colomer et al., 2003; Serra et al., 2002). Characterizing turbulent plumes generated by high-temperature lacustrine hydrothermal systems is of interest since plume-driven buoyancy flux, momentum flux, and turbulent mixing with ambient waters may be important to the chemical (e.g., Varekamp et al., 2000) and buoyancy budgets of a lake.

Yellowstone Lake, a large (~341 km^2) alpine lake (2,357-m altitude) located in Yellowstone National Park (44°28′N, 110°22′W) in northwestern Wyoming, USA (Figure 1), is a hydrothermally active lake that straddles the southeastern boundary of the 640-ka Yellowstone caldera. The northern, intracaldera, portion of the lake hosts a multitude of thermal features, including explosion craters, siliceous spires, and more than 250 vents (Morgan et al., 2003). The three largest hydrothermal fields (Figure 1) are located in West Thumb basin, in the Mary Bay explosion crater complex, and to the southeast of Stevenson Island. The Stevenson Island vent field, commonly referred to as the "Deep Hole" site because it is located in the deepest part of the lake (~110–120 m), was comprehensively monitored using submersible, geophysical, and geochemical instrumentation from 2016–2018 during fieldwork for the Hydrothermal Dynamics of Yellowstone Lake project (Sohn et al., 2017). The Deep Hole hosts a vapor-dominated acid-sulfate (pH ~ 4.3) system where hydrothermal fluids, with dilute compositions of condensed steam with minor components (~1%) of volcanic gas (CO_2 and H_2S), discharge into the water column at high temperatures. Fluid temperatures measured a few centimeters beneath the lake floor reach the ambient boiling point of ~174 °C (Fowler et al., 2019).

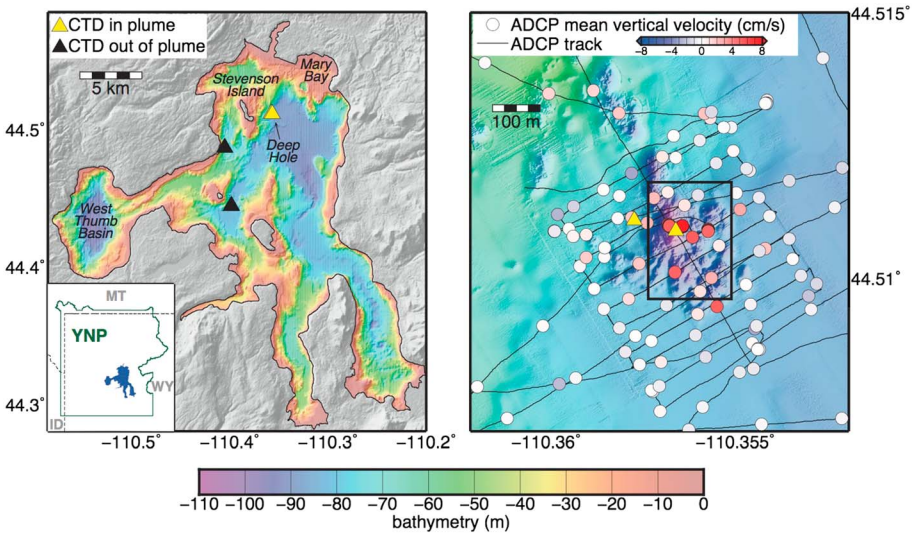

Figure 1. (a) Bathymetry of Yellowstone Lake, within Yellowstone National Park (YNP), showing location of conductivity-temperature-depth (CTD) profiles used in this study. Two CTD profiles were collected at each site. (b) Bathymetry of Deep Hole hydrothermal vent field, Acoustic Doppler current profiler (ADCP) tracks and CTD profile locations used in this study. Colored circles indicate the depth-averaged vertical water column velocity along the ADCP survey. Black box delineates extent of region for ADCP vertical velocity profile averages in Figure 3.

Discharge occurs through small, discrete vents that are distributed across a ~200 × 200-m area characterized by a dense set of superposed pockmarks in the lake floor sediments (Figure 1).

In this paper, we describe conductivity-temperature-depth (CTD) and acoustic Doppler current profiler (ADCP) measurements made in and around the Deep Hole site in August 2018. These water column data constrain the neutral height (depth horizon at which the plume fluids have the same density as the ambient water) and vertical velocity profile of the turbulent plume generated by the sublacustrine hydrothermal system during late summer, when the water column was near its annual peak in stratification. We use a plume model to estimate the boundary conditions at the lake floor that best reproduce our water column observations, which yields estimates of the buoyancy, heat, and mass fluxes of the hydrothermal field.

2. Data and Methods

ADCP and CTD data were collected in Yellowstone Lake from 2–16 August 2018, aboard the R/V *Annie II*. CTD data used in this study were collected using a *Seabird SBE19plusV2* sensor mounted on the remotely operated vehicle (ROV) *Yogi*. Profiles were collected during the initial descent of remotely operated vehicle Yogi as it dove to perform a variety of tasks on the lake floor at the hydrothermal site, including instrument recovery and sample acquisition. Raw data (4 Hz) were low-pass filtered (1.0-s corner period for depth and pressure and 0.5-s corner period for temperature, conductivity, and dissolved oxygen), and the temperature and dissolved oxygen were lag corrected relative to the conductivity and depth measurements following manufacturer recommendations prior to averaging all data into 0.5-m bins.

Comparison of six CTD profiles acquired on 12 August 2018 (Figure 1) reveals the presence of a salinity anomaly in the water column above the Deep Hole hydrothermal site. Profiles from the hydrothermal site exhibit reduced salinities over a depth range from ~35–55 m, with a distinct minima at a depth of ~45 m, compared to profiles acquired well outside the hydrothermal area (Figure 2). We interpret the depth interval over which the salinity anomaly is observed as the plume's neutral height—that is, the level where the plume spreads laterally because the modified plume waters have the same density as the ambient medium (Morton et al., 1956; Turner, 1979). Lateral spreading at the neutral height expands the plume footprint in the water column compared to the footprint of the buoyant plume stem, making it a natural target for plume surveys in marine environments (e.g., Baker et al., 1995). The salinity anomaly at the plume's neutral height is approximately −0.0014 psu or ~5% of ambient values. While hydrothermal fluids at the Deep Hole site are

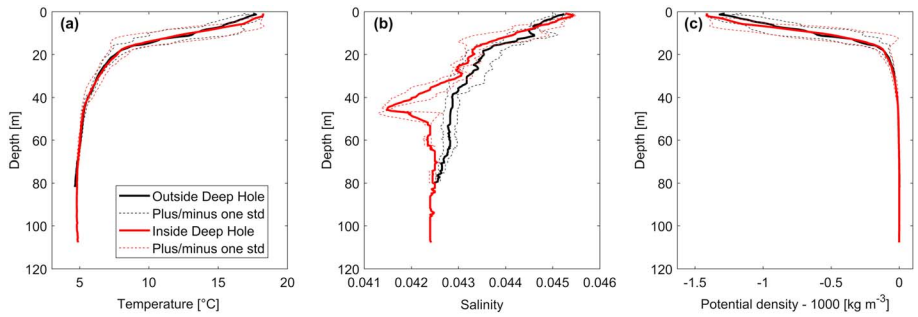

Figure 2. Conductivity-temperature-depth profiles. (a) Temperature, (b) salinity, and (c) potential density collected on 12 August 2018. Average values and standard deviation for four profiles collected outside the hydrothermal area are shown in black and for two profiles from the hydrothermal area in red.

chemically similar to lake water for many dissolved constituents, they exhibit Cl concentrations that are reduced by as much as 17% relative to ambient lake water (Fowler et al., 2019). Since Cl is a conservative species, salinity provides a useful plume tracer.

ADCP data, acquired using a pole-mounted, downward-looking 300-kHz *RDI Navigator* system rigidly affixed to the R/V Annie II, constrain the size and vertical velocity of the buoyant plume. Two survey modes were used: opportunistic underway sampling based on other cruise priorities and a dedicated radiator survey to constrain the plume structure (see supporting information S1 for details). During opportunistic sampling, upward velocities of a few to over 10 cm/s were observed in the vicinity of the Deep Hole region (Figures 1b and 3a). Just outside the hydrothermal field, the vertical velocities tended to be weakly negative (Figure 3a), possibly indicating a plume-driven recirculation cell. The strongest upwelling velocities (in excess of 10 cm/s) were observed on 13 August, and a secondary peak in the vertical velocity in the upper water column (~18-m depth) was also observed at this time. All observations of the shallow secondary peak were within ~100 m of each other, but since these data were not acquired as part of a coordinated survey, the spatial characteristics of the upper water column signal are poorly constrained.

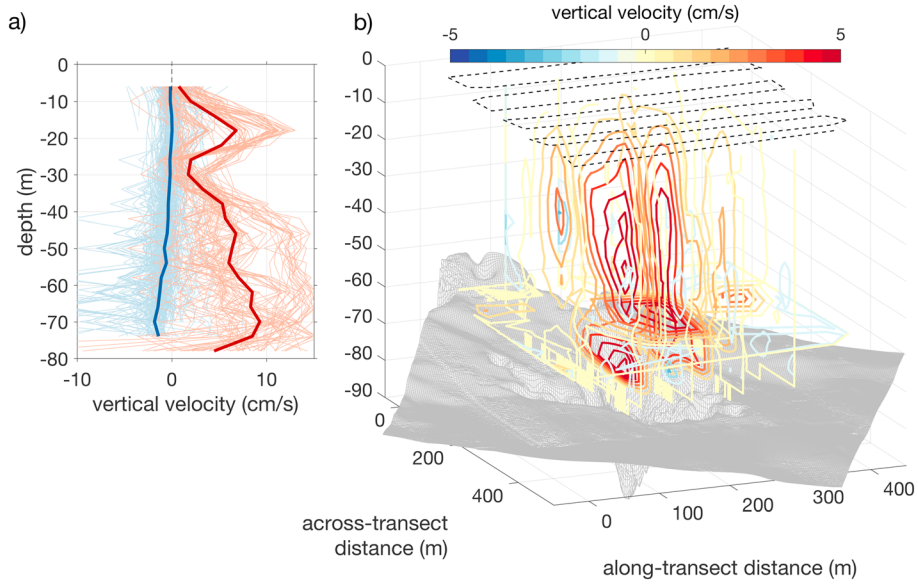

Figure 3. (a) Vertical velocity profiles taken on 13 and 14 August 2018 from within a 175 m by 250 m (EW by NS) box centered over the Deep Hole region (Figure 1) in red and profiles outside this geographic range in blue. Average profiles are shown in bold. Small, negative velocities at the bottom of the profiles taken outside the plume are suggestive of a localized convection cell. (b) Plume vertical velocity (contours) as sampled during the radiator survey on 14 August 2018. Vertical planes are located at 75-m intervals in the along-track direction; the horizontal plane is located at 60-m depth. Bathymetry shown in gray. Note that the deepest parts of the lake floor at ~120 m extend beyond the vertical axis. Vertical exaggeration is 5×.

During the radiator survey on 14 August, peak upward velocities were somewhat weaker at ~8 cm/s, and the secondary peak in the upper water column was not observed (Figure 3b). Upwelling velocities over the Deep Hole exhibited a diffuse maximum near ~50-m depth that was roughly centered over the deepest region (Figure 3b). The lateral scale of the primary plume has an extent of approximately 150–200 m and is roughly axisymmetric with little observed spreading in height. A weaker upwelling region on the scale of ~50 m is observed at the periphery of the primary feature, perhaps a manifestation of distributed venting. The vertical velocity decays above the thermocline. Interpretation of small-scale structure at depth is restricted by beam spreading of the ADCP, which is ~90 m at 80-m depth.

The horizontal currents were generally of the same magnitude as the vertical velocity in the plume, but the signal is considerably more complex, with significant spatiotemporal variability and veering of currents in depth (Figure S1). The complexity of the horizontal currents may be due to the background circulation, for example, seiches (Luttrell et al., 2013) and wind-generated internal waves (Wuest & Lorke, 2003), or interaction between the plume and the ambient circulation. Additional observations will be required to resolve this issue, as existing measurements do not resolve motions at the local buoyancy period (~2.5 min in thermocline compared to 2-min ensemble averaging) and are space-time aliased at longer time scales corresponding to seiche periods (dominant mode of 78 min compared to ~2-hr radiator survey duration).

3. Plume Modeling

The behavior of turbulent plumes in stratified media (Morton et al., 1956) is relevant to a variety of geological and environmental processes (e.g., Woods, 2010, and references therein), and hydrothermal plumes generated by deep-sea vent fields have been studied extensively (e.g., Baker et al., 1995, and references therein). Modeling hydrothermal plumes in the marine environment requires consideration of both the solutal and thermal contributions to fluid density (Speer & Rona, 1989; Turner & Campbell, 1987), and we use the plume model described by Stranne et al. (2010) to simulate the rise of a turbulent plume at the Deep Hole site. The model conserves heat, mass, salinity, and momentum, uses an equation of state appropriate for freshwater environments (Chen & Millero, 1986), and uses the observed salinity and potential temperature profiles to define the ambient medium. This approach allows us to use the observed magnitude of the minimum salinity anomaly (−0.0014 psu), along with the neutral height itself, as modeling constraints.

The initial salinity of the plume fluids, S_0, is constrained to be 0.03 psu by chemical analysis of hydrothermal fluid samples (Fowler et al., 2019). The initial area of the plume, A_0, is estimated as 54,000 m^2 based on the size of the pockmark field created by hydrothermal discharge. The initial plume depth, D_0, is set at 115 m, which is the mean value of the vents sampled during Hydrothermal Dynamics of Yellowstone Lake fieldwork (full range of 109–117 m). The ambient temperature and salinity profiles were defined by averaging four CTD casts taken from two sites well away from the hydrothermal area (Figures 1a and 2). The ambient potential density and salinity profiles were extrapolated (nearest-neighbor) to 120-m depth since they did not extend to the depth of the Deep Hole hydrothermal field. Note that gradients in the deep parts of the lake are very weak (Figure 2).

The initial temperature (T_0) and vertical velocity (W_0) of the plume were allowed to vary, and we used a multidimensional, unconstrained, nonlinear minimization technique (Nelder-Mead method, Lagarias et al., 1998) to find combinations of T_0 and W_0 matching our observational constraints: the plume neutral buoyancy height and salinity anomaly (−0.0014 psu). The neutral buoyancy height equals 70 m for a 115-m deep source given the observed neutral depth of 45 m. The method yields parameter estimates of $T_0 = 9.5$ °C and $W_0 = 2.6 \times 10^{-3}$ cm/s with misfits of 0.03 mm for the neutral buoyancy height and 5×10^{-6} psu for the salinity anomaly (Figure 4). With these model parameters, the site has buoyancy, mass, and heat fluxes of 3.2×10^{-3} m^4/s^3, 1.4×10^3 kg/s, and 28 MW, respectively.

We did not use the plume's velocity field to constrain the model, but our best fitting model yields vertical velocities of ~10 cm/s in the mid-water column that decrease to essentially 0 at a depth of 30 m, similar to the 1-D average values observed within the hydrothermal field (Figure S4). The modeled plume overshoots the neutral height by ~15 m due to an excess of momentum, and the ADCP profiles appear to capture this overshoot. The positive vertical velocities observed at shallow depths within the thermocline on 13 August (Figure 3a) are above the top of the plume and seem to require a different source mechanism.

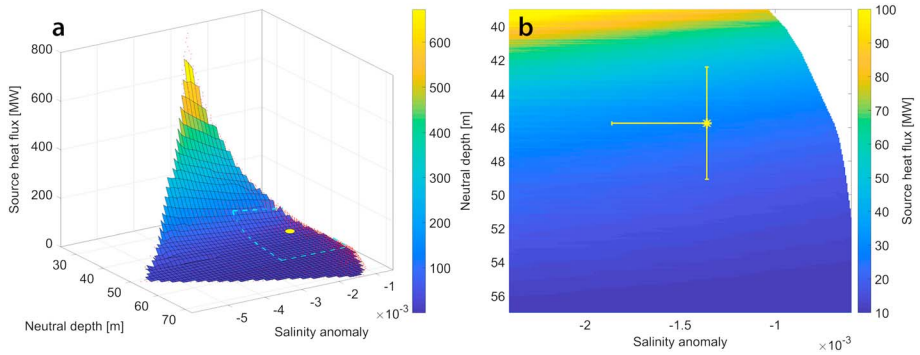

Figure 4. (a) Solution space as a fitted surface (using cubic interpolation) to the model results (red dots). A few thousand simulations were run using the baseline model assumptions and different combinations of T_0 (ranging between 5 and 16 °C) and W_0 (ranging between 3×10^{-4} and 3×10^{-2} cm/s). Yellow dot represents the observed neutral depth and salinity anomaly. (b) Enlarged, planar view of the solution space defined by cyan box in panel (a). The observed neutral depth and salinity anomaly are shown as a yellow asterisk with error bars corresponding to ±3.3 m and $+1 \times 10^{-4}$ psu, respectively. The heat flux for the solution space delineated by these values varies between 20 and 50 MW.

The formal uncertainty of these flux estimates is primarily due to uncertainty in the neutral height estimate (see discussion of sensitivity tests below and in the supporting information S2). During our survey period, isotherms at the neutral depth interval observed on a nearby thermistor chain had vertical excursions of ±~3 m (~12- to 13-hr period oscillations), and the salinity anomalies observed in the CTD data from the hydrothermal area can be approximated as Gaussian with a mean depth of 45 m and a standard deviation of 3.3 m. For modeling purposes, we therefore parameterize the plume's neutral height as 70 ± 3.3 m to one standard deviation. The model solution space yields heat flux values of 20–45 MW within this range (Figure 4b). The model is less sensitive to the magnitude of the salinity anomaly (see supporting information S2 for discussion), which is ~3× the nominal resolution of the CTD conductivity sensor. Uncertainties related to the model salinity anomaly most likely arise due to undersampling, since none of our CTD profiles sampled the buoyant plume stem. In contrast, the model output represents an average taken over the plume radius at the neutral height, so it seems likely that our CTD data underestimates the radially averaged anomaly (Stranne et al., 2010). If this value is underestimated by 25% (one increment of instrument resolution, ~0.0005 psu), then the maximum heat plume heat flux increases to 50 MW (Figure 3b).

We can compare the buoyancy flux from our best fitting numerical model against an approximate scaling law for the plume neutral height (Turner, 1979). The plume neutral height is given by

$$H_N = 2.1(\pi f_0)^{1/4} N^{-3/4} \quad (1)$$

where H_N is the neutral height, f_0 is the source buoyancy flux, and N is the Brunt-Vaisalla frequency. If we calculate the Brunt-Vaisalla frequency over the depth interval from 115–25 m (extending ~20 m above the observed neutral height), $N = 2.0 \times 10^{-3}$ rad/s and a buoyancy flux of 3.2×10^{-3} m^4/s^3 yields the observed neutral height (70 m), matching the result from our plume model. The scaling law analysis is thus consistent with our plume modeling results, but it is sensitive to the depth interval over which the density gradient is calculated (see supporting information Figure S5).

4. Results and Discussion

We present CTD and ADCP data demonstrating that the Deep Hole hydrothermal system located on the floor of Yellowstone Lake to the southeast of Stevenson Island generates a water column plume. Our observations constrain the plume's neutral height, salinity anomaly at the neutral height, and vertical velocity profile at the time of our surveys, when the lake was near its annual peak in stratification. We use a plume model to constrain the hydrothermal discharge fluxes that reproduce the observed water column anomalies and find that the model results are consistent with a simple scaling law for the plume neutral height. Our best fitting model has heat, mass, and buoyancy fluxes of 28 MW, 1.4×10^3 kg/s, and ~3.2×10^{-3} m^4/s^3, respectively. These flux estimates are ~3× greater than previous estimates for the total hydrothermal mass flux into the lake based on mass-balance calculations for Cl (Balistrieri et al., 2007). Considering that the

Deep Hole site is one of at least three major hydrothermal fields in Yellowstone Lake (including Mary Bay and West Thumb, Figure 1a), our results suggest that hydrothermal fluxes into the lake may be considerably larger than previously recognized. Our heat flux estimate yields an average flux of ~500 W/m^2 over the spatial extent of the Deep Hole pockmark field. While this heat flux is spatially limited, it is significantly larger than the daily average surface flux, which peaks at values of ~200 W/m^2 in July, suggesting that hydrothermal inputs may play a significant, but as of yet poorly understood, role in the lake's thermal and buoyancy budgets.

The Deep Hole hydrothermal field is an acid-sulfate, vapor-dominated system (Fowler et al., 2019), and our results indicate it may be one of the largest such systems in Yellowstone. In aggregate, acid-sulfate hydrothermal fields cover an area of ~35 km^2 on the Yellowstone Plateau (Rodman et al., 1996; Werner & Brantley, 2003), but heat flux estimates are only available for two subaerial fields: 11.8 ± 1.4 MW for the Obsidian Pool Thermal Area at Mud Volcano (just north of Yellowstone Lake) and 8.8 ± 0.4 MW for the Solfatara Plateau Thermal Area (Hurwitz et al., 2012). Heat flux at the Deep Hole field is thus estimated to be ~2–3× greater than these subaerial fields, but the paucity of data emphasizes the uncertainties inherent to our understanding of heat flow on the Yellowstone Plateau.

We ran a series of sensitivity tests to assess the formal uncertainties of our plume model (see supporting information S1). The principal result of these tests is that our source flux estimates are most sensitive to the source depth, D_0, assumption, because it directly impacts the estimate of the plume's neutral height (for a given neutral depth). This high degree of sensitivity is illustrated in equation (1), which relates the buoyancy flux to the neutral height to the fourth power. By contrast, our results are insensitive to the assumed source area, A_0, because area variations are balanced by initial velocity, W_0, variations, such that the plume fluxes remain nearly constant. When these quantifiable uncertainties are considered, we find that the Deep Hole heat flux could range from 20 to 50 MW.

Our model simplifies several aspects of the plume physics, primarily because we lack the observations required to constrain more complex simulations. For example, the distributed nature of hydrothermal discharge on the lake floor could affect the plume's dynamic behavior. A distributed hydrothermal source can create a disorganized plume structure (Bemis et al., 2002) and can cause plume isosurfaces to initially contract into a mixing layer before expanding as the plume rises further (Bemis et al., 2002; Epstein & Burelbach, 2001). However, beam spreading of the ADCP precluded the observation of any such effect in our data. The interaction of the buoyant plume with other processes, such as basin-scale circulation, seiches, and baroclinic motions, is an intriguing topic, but our survey data lack the spatiotemporal resolution required to resolve these processes (see supporting information S1 for discussion). Buoyant plumes are known to generate internal waves in stratified fluids, including the atmosphere and ocean, through a variety of mechanisms (e.g., Ansong & Sutherland, 2010; Ezhova et al., 2016; Fritts & Alexander, 2003; Lecoanet et al., 2015). These processes may also be active in lakes, where the enclosed geometry may introduce additional complexities, such as plume-induced stratification perturbations and forcing of basin-scale seiches.

Overall, the lacustrine environment provides a more complex medium for buoyant plumes relative to the deep sea, where most hydrothermal plume studies have been conducted. Our results motivate future work to understand how lacustrine hydrothermal systems affect, and interact with, ambient hydrodynamic processes. The acquisition of spatially and temporally more comprehensive survey data is required to address these issues, and more complex models (e.g., distributed source, temporal variations in plume flux, and ambient stratification) may be necessary.

5. Conclusions

1. The Deep Hole hydrothermal system, located at lake floor depths of ~115 m to the Southeast of Stevenson Island, generates a water column plume in Yellowstone Lake. During our observational period, when the water column was near peak summer stratification, the plume had vertical velocities of up to ~10 cm/s in the mid-water column and generated a salinity anomaly of −0.0014 psu (5% lower than background) at a neutral buoyancy depth of ~45 m, corresponding to a rise height of ~70 m.
2. Our numerical model can match the plume's salinity anomaly and neutral height to within measurement error. In our best fitting model the hydrothermal system has an advective heat flux of 28 MW and a mass flux of 1.4 × 10^3 kg/s. These flux estimates are 2–3× larger than previous estimates for hydrothermal

fluxes into the lake, indicating hydrothermal processes may play a larger role in the lake's hydrologic balance than previously appreciated.

3. he impact of hydrothermal plumes on the hydrodynamic behavior of volcanic lakes is poorly understood, and additional observations will be required to gain insight into this issue.

Acknowledgments
The authors thank Yellowstone National Park Fisheries and Aquatic Sciences, The Global Foundation for Ocean Exploration, and Paul Fucile for logistical support. This research was supported by the National Science Foundation grants EAR-1516361 to R. S., EAR-1514865 to K. L., and EAR-1515283 to R. H. and J. F. All work in Yellowstone National Park was completed under an authorized Yellowstone research permit (YELL-2018-SCI-7018). CTD and ADCP profiles reported in this paper are available through the Marine Geoscience Data System (doi:10.1594/IEDA/324713 and doi:10.1594/IEDA/324712, accessed last on 17 April 2019, respectively).

References

Ansong, J. K., & Sutherland, B. R. (2010). Internal gravity waves generated by convective plumes. *Journal of Fluid Mechanics*, *648*, 405–434. https://doi.org/10.1017/S0022112009993193

Baker, E. T., German, C. R., & Elderfield, H. (1995). Hydrothermal plumes over spreading-center axes: Global distributions and geological inferences. In S. Humphris, R. Zierenberg, L. S. Mullineaux, & R. Thomson (Eds.), *Seafloor hydrothermal systems: Physical, chemical, biological, and geological interactions*, *Geophys. Monogr. Ser., 91* (pp. 47–71). Washington DC: AGU.

Balistrieri, L. S., Shanks, W. C. III, Cuhel, R. L., Aguilar, C., & Klump, J. V. (2007). The influence of sublacustrine hydrothermal vents on the geochemistry of Yellowstone Lake. In L. A. Morgan (Ed.), *Integrated geoscience studies in the greater Yellowstone area—Volcanic, tectonic, and hydrothermal processes in the Yellowstone Geoecosystem: U. S*, (Vol. 1717, pp. 169–199). Geological Survey Professional Paper.

Bemis, K. G., Rona, P. A., Jackson, D., Jones, C., Silver, D., & Mitsuzawa, K. (2002). A comparison of black smoker hydrothermal plume behavior at Monolith Vent and at Clam Acres Vent Field: Dependence on source configuration. *Marine Geophysical Research*, *23*, 81–96.

Chen, C.-T. A., & Millero, F. J. (1986). Thermodynamic properties for natural waters covering only the limnological range 1. *Limnology and Oceanography*, *31*(3), 657–662.

Colomer, J., Serra, T., Piera, J., Roget, E., & Casamitjana, X. (2001). Observations of a hydrothermal plume in a karstic lake. *Limnology and Oceanography*, *46*(1), 197–203.

Colomer, J., Serra, T., Soler, M., & Casamitjana, X. (2003). Hydrothermal plumes trapped by thermal stratification. *Geophysical Research Letters*, *30*(21), 2092. https://doi.org/10.1029/2003GL018131

Crane, K., Hecker, B., & Golubev, V. (1991). Hydrothermal vents in Lake Baikal. *Nature*, *350*, 281.

Dymond, J., Collier, R. W., & Watwood, M. E. (1989). Bacterial mats from Crater Lake, Oregon and their relationship to possible deep-lake hydrothermal venting. *Nature*, *342*, 673–675.

de Ronde, C. E. J., Stoffers, P., Garbe-Schonberg, D., Christenson, B. W., Jones, B., Manconi, R., et al. (2002). Discovery of active hydrothermal venting in Lake Taupo, New Zealand. *Journal of Volcanology and Geothermal Research*, *115*, 255–273.

Epstein, M., & Burelbach, J. P. (2001). Vertical mixing above a steady circular source of buoyancy. *International Journal of Heat and Mass Transfer*, *44*, 525–536.

Ezhova, E., Cenedese, C., & Brandt, L. (2016). Interaction between a vertical turbulent jet and a thermocline. *Journal of Physical Oceanography*, *46*. https://doi.org/10.1175/JPO-D-16-0035.1

Fowler, A. P. G., Tan, C., Cino, C., Scheuermann, P., Volk, M. W. R., Shanks, P. III, & Seyfried, W. E. Jr. (2019). Vapor-driven sublacustrine vents in Yellowstone Lake, Wyoming, USA. *Geology*. https://doi.org/10.1130/G45577.1

Fritts, D. C., & Alexander, M. J. (2003). Gravity wave dynamics and effects in the middle atmosphere. *Reviews of Geophysics*, *41*(1), 1003. https://doi.org/10.1029/2001RG000106

Hurwitz, S., Harris, R. N., Werner, C. A., & Murphy, F. (2012). Heat flow in vapor dominated areas of the Yellowstone Plateau volcanic field: Implications for the thermal budget of the Yellowstone Caldera. *Journal of Geophysical Research*, *117*, B10207. https://doi.org/10.1029/2012JB009463

Klump, J. V., Remsen, C. C., & Kaster, J. L. (1988). The presence and potential impact of geothermal activity on the chemistry and biology of Yellowstone Lake, Wyoming. In M. DeLuca, & I. Babb (Eds.), *Global venting, midwater and benthic ecological processes*, NOAA National Undersea Research Program Research Report no. 88-4, (pp. 81–98).

Lagarias, J. C., Reeds, J. A., Wright, M. H., & Wright, P. E. (1998). Convergence properties of the Nelder–Mead simplex method in low dimensions. *SIAM Journal on Optimization*, *9*(1), 112–147.

Lecoanet, D., Le Bars, M., Burns, K. J., Vasil, G. M., Brown, B. P., Quataert, E., & Oishi, J. S. (2015). Numerical simulations of internal wave generation by convection in water. *Physical Review E*, *91*. https://doi.org/10.1103/PhysRevE.91.063016

Luttrell, K., Mencin, D., Francis, O., & Hurwitz, S. (2013). Constraints on the upper crustal magma reservoir beneath Yellowstone Caldera inferred from lake-seiche induced strain observations. *Geophysical Research Letters*, *40*, 501–506. https://doi.org/10.1002/grl.50155

Morgan, L. A., Shanks, W. C., Lovalvo, D. A., et al. (2003). Exploration and discovery in Yellowstone Lake: Results from high-resolution sonar imaging, seismic reflection profiling, and submersible studies. *Journal of Volcanology and Geothermal Research*, *122*, 221–242. https://doi.org/10.1016/S0377-0273(02)00503-6

Morton, B., Taylor, G. I., & Turner, J. S. (1956). Turbulent gravitational convection from maintained and instantaneous sources. *Proceedings of the Royal Society of London. Series A*, *234*, 1–24.

Rodman, A., Shovic, H., & Thoma, D. (1996). *Soils of Yellowstone National Park*. Yellowstone Center for Resources, National Park Service.

Serra, T., Colomer, J., Gacia, E., Soler, M., & Casamitjana, X. (2002). Effects of a turbid hydrothermal plume on the sedimentation rates in a karstic lake. *Geophysical Research Letters*, *29*(21), 2029. https://doi.org/10.1029/2002GL015368

Sohn, R., Harris, R., Linder, C., Luttrell, K., Lovalvo, D., Morgan, L., et al. (2017). Exploring the restless floor of Yellowstone Lake. *Eos*, *98*. https://doi.org/10.1029/2017EO087035

Speer, K. G., & Rona, P. A. (1989). A model of an Atlantic and Pacific hydrothermal plume. *Journal of Geophysical Research*, *94*(C5), 6213–6220.

Stranne, C., Sohn, R. A., Liljebladh, B., & Nakamura, K. (2010). Analysis and modeling of hydrothermal plume data acquired from the 85°E segment of the Gakkel Ridge. *Journal of Geophysical Research*, *115*, C06028. https://doi.org/10.1029/2009JC005776

Tiercelin, J.-J., Pflumio, C., Castrec, M., Boulegue, J., Rolet, J., Coussement, C., et al. (1993). Hydrothermal vents in Lake Tanganyika, East African Rift System. *Geology*, *21*, 499–502.

Turner, J. S. (1979). *Buoyancy effects in fluids*. Cambridge, UK: Cambridge University Press.

Turner, J. S., & Campbell, I. H. (1987). Temperature, density, and buoyancy fluxes in "black smoker" plumes, and the criterion for buoyancy reversal. *Earth and Planetary Science Letters*, *86*, 85–92.

Varekamp, J. C., Pasternack, G. B., & Rowe, G. L. Jr. (2000). Volcanic lake systematics II. Chemical constraints. *Journal of Volcanology and Geothermal Research*, *97*, 161–179.

Werner, C., & Brantley, S. (2003). CO2 emissions from the Yellowstone volcanic system. *Geochemistry, Geophysics, Geosystems*, *4*(7), 1061. https://doi.org/10.1029/2002GC000473

Woods, A. W. (2010). Turbulent plumes in nature. *Annual Reviews of Fluid Mechanics*, *42*, 391–412. https://doi.org/10.1146/annurev-fluid-121108-145430

Wuest, A., & Lorke, A. (2003). Small-scale hydrodynamics in lakes. *Annual Review of Fluid Mechanics*, *35*, 373–412. https://doi.org/10.1146/annurev.fluid.35.101101.161220